Inorg. Chem. **2007**, *46*, 72–78

Design of Molecular Scaffolds Based on Unusual Geometries for Magnetic Modulation of Spin-Diverse Complexes with Selective Redox Response

Maurício Lanznaster,[†,||] Mary Jane Heeg,[†] Gordon T. Yee,[‡] Bruce R. McGarvey,*[,§] and Claudio N. Verani*[,†]

Department of Chemistry, Wayne State University, 5101 Cass Avenue, Detroit, Michigan 48202, Department of Chemistry, Virginia Polytechnic Institute and State University, 107 Davidson Hall, Blacksburg, Virginia 24061, and Department of Chemistry and Biochemistry, University of Windsor, 401 Sunset Avenue, Windsor ON N9B 1P4, Canada

Received May 30, 2006

A weakly coupled heterometallic [CuFe] complex has been prepared in which the metal centers are coordinated to a new electroactive ligand. The spin-diverse system delivers distinct ground states upon application of selective redox potentials. Ligand oxidation fosters radical generation, and the initial ground state associated with a weakly coupled [CuFe] core switches to a ground state associated with the [Fe–radical] coupling; the Cu(II) ion remains uncoupled. A third state is obtained upon reduction of the cupric center and in absence of the radical. The possibilities and limitations of these systems are discussed.

Introduction

Research in molecular electronics gives considerable importance to molecules able to behave as switches when deposited onto surfaces.[1,2] Our group is focusing efforts toward a modular platform in which surface-anchored units connect to redox-active spin-diverse terminal units via metal bridges (Scheme 1). Control over the oxidation states of these redox-active modules can lead to the understanding of relationships between electronic and magnetic behavior associated with the number and nature of each spin carrier present.[3] Heterometallic assemblies pave the road to molecular arrays based on exchange coupling between metal ions, and the current leading design is based either on a building block approach[4] or on fused hybrid ligands.[5,6] Similarly, considerable effort has been devoted to the use of transition metal complexes with electroactive ligands capable of stabilizing organic radicals (L → L$^{\bullet}$).[7−17] In this approach, semiquinone,[8] verdazyl,[9] phenoxyl,[10] nitronyl-nitroxide,[11] and

Scheme 1

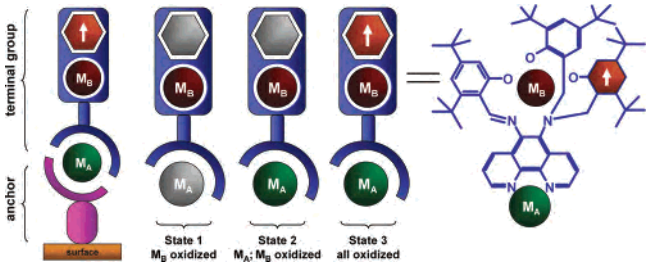

* To whom correspondence should be addressed. E-mail: cnverani@chem.wayne.edu.
[†] Wayne State University.
[‡] Virginia Polytechnic Institute and State University.
[§] University of Windsor.
[||] Present address: Institute of Chemistry, Universidade Federal Fluminense, Niterói, Rio de Janeiro 24020-150, Brazil.

(1) (a) Park, J.; Pasupathy, A. N.; Goldsmith, J. I.; Chang, C. Yaish, Y.; Petta, J. R.; Rinkoski, M.; Sethna, J. P.; Abruna, H. D.; McEuen, P. L.; Ralph, D. C. *Nature* **2002**, *417*, 722. (b) Gittins, D. I.; Bethell, D.; Schiffrin, D. J.; Nichols, R. J. *Nature* **2000**, *408*, 67.
(2) (a) Wassel, R. A.; Gorman, C. B. *Angew. Chem., Int. Ed.* **2004**, *43*, 5120. (b) Joachim, C.; Gimzewski, J. K.; Aviram, A. *Nature* **2000**, *408*, 541.
(3) Shultz, D. A.; Bodnar, S. H.; Vostrikova, K. E.; Kampf, J. W. *Inorg. Chem.* **2000**, *39*, 6091−6093.
(4) Chaudhuri, P. *Coord. Chem. Rev.* **2003**, *243* (1−2), 143.
(5) (a) Vannelli, T. A.; Karpishin, T. B. *Inorg. Chem.* **2000**, *39*, 340. (b) Vannelli, T. A.; Karpishin, T. B. *Inorg. Chem.* **1999**, *38*, 2246.
(6) (a) Goslinski, T.; Zhong, C.; Fuchter, M. J.; Stern, C. L.; White, A. J. P.; Barrett, A. G. M.; Hoffman, B. M. *Inorg. Chem.* **2006**, *45*, 3686 and references therein. (b) Zhao, M.; Stern, C.; Barrett, A. G. M.; Hoffman, B. M. *Angew. Chem., Int. Ed.* **2003**, *42*, 462.
(7) (a) Dei, A.; Gatteschi, D.; Sangregorio, C.; Sorace, L. *Acc. Chem. Res.* **2004**, *37*, 827 and references therein.
(8) Pierpont, C. G. *Coord. Chem. Rev.* **2001**, *219−221*, 415.
(9) (a) Mukai, K. In *Magnetic Properties of Organic Materials*; Lahti, P. M., Ed.; Marcel Dekker: New York, 1999; pp 103−125. (b) Hicks, R. G.; Lemaire, M. T.; Oehrstroem, L.; Richardson, J. F.; Thompson, L.; Xu, Z. *J. Am. Chem. Soc.* **2001**, *123*, 7154.

10.1021/ic060944a CCC: $37.00
Published on Web 12/06/2006

Scheme 2

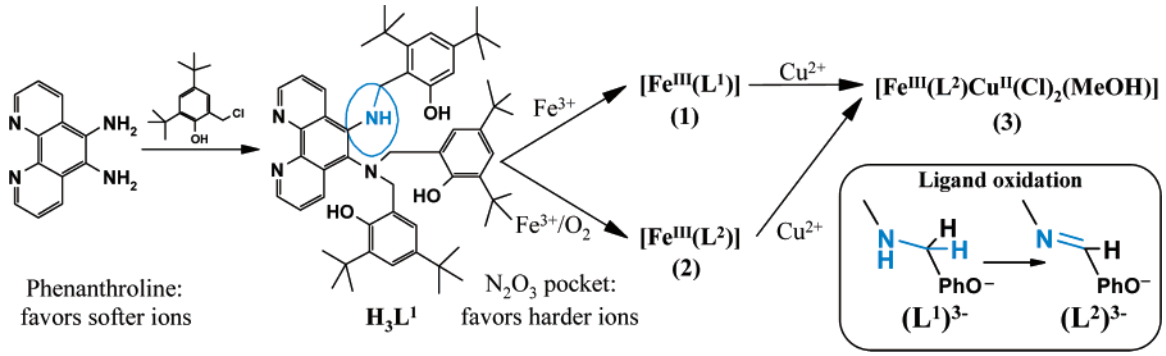

aminyl[12] radicals are generated by applying proper potentials via electrochemical methods. These radicals can couple to one or more paramagnetic metal centers when properly arranged in a coordination complex. In absence of a potential that triggers radical formation, the metal complex rests in its "metal-only" ground state. The application of specific potentials promotes radical formation, and the molecule then adopts a coupled "metal−radical" ground state. The approaches toward radical-mediated ground-state switching were pioneered by Gatteschi,[13] Pierpont,[14] and Hendrikson,[15] being expanded recently to uncoupled $[M_A-L-M_A]$ cores that become strongly coupled $[M_A-L^{\bullet}-M_A]$ upon generation of bridging benzenyl radicals.[16,17]

In this account, we report on the monometallic complex $[Fe^{III}L^1]$ **(1)** that is oxidized to $[Fe^{III}L^2]\cdot{}^1/_2MeCN$ **(2)** and serves as a precursor for bimetallic $[Fe^{III}(L^2)Cu^{II}(Cl)_2(MeOH)]$ **(3).** These species are based on the newly developed binucleating and electroactive ligand $\mathbf{H_3L^1}$ (Scheme 2), which will be used as a terminal module for redox-driven surface chemistry. The design of the ligand takes advantage of our recent observation that five-coordinate trivalent ions appear to enhance the formation and reversibility of phenolate/phenoxyl processes in the cyclic voltammetric time scale.[18] The redox response of spin-diverse **3** is based on controlled oxidations and reductions of its fundamental components (i.e., the metal centers and the electroactive arms of the ligand). We observe that specific potentials trigger definite responses, described as states 1−3 in Scheme 1. Each of these states is equivalent to alterations of the spin ground states measured by EPR spectroscopy.

Experimental Section

Materials and Methods. Reagents and solvents were used as received from commercial sources, unless otherwise noted. Dichloromethane and acetonitrile were doubly purified using alumina columns in a solvent purification system from Innovative Technologies, and methanol was distilled over CaH_2. Infrared spectra were measured from 4000 to 400 cm^{-1} as KBr pellets on a Tensor 27 FTIR-Spectrophotometer. ^1H NMR spectra were measured using Varian 300 and 400 mHz instruments. ESI(positive) spectra were measured in either a triple-quadrupole Micromass QuattroLC or in a single-quadrupole Waters ZQ2000 mass spectrometer with an electrospray/APCI or ESCi source. Experimental assignments were simulated on the basis of peak position and isotopic distributions. Elemental analyses were performed by Midwest Microlab, Indianapolis, IN. Cyclic voltammetry experiments were performed using a BAS 50W voltammetric analyzer. A standard three-electrode cell was employed with a glassy-carbon working electrode, a Pt-wire auxiliary electrode, and an Ag/AgCl reference electrode under an inert atmosphere at room temperature (RT). Potentials are presented versus Fc^+/Fc[19] as the internal standard. First derivative X-band EPR spectra of 1.0×10^{-3} M acetone solutions of **2** and **3** were performed with a Bruker ESP 300 spectrometer at 115 K using liquid nitrogen as the coolant. Manipulations of EPR spectra were done using the WINEPR suite from Bruker. Simulations of powder EPR spectra of Fe(III) were obtained using a program supplied by Dr. A. Ozarowski, Florida State University, Tallahassee, FL. Simulations of Cu(II) spectra used a program written by Prof. B.R. McGarvey, whereas simulations of the spin coupled $[Fe^{III}-Cu^{II}]$ core used a program supplied by Dr. H. Weihe, University of Copenhagen, Denmark. Magnetic measurements as a function of temperature were performed from 1.8 to 300 K for **3** on a 5- or 7-T Quantum Design MPMS SQUID magnetometer. Diamagnetic corrections used Pascal's constants, and the diamagnetic susceptibility of the sample holder was also taken into account.

Syntheses. H_3L^1. The ligand *N*,*N*,*N*′-tris-(3,5-di-tert-butyl-2-hydroxybenzyl)-[1,10]-phenanthroline-5,6-diamine was prepared by a procedure previously reported for the synthesis of *N*,*N*,*N*′-tris-(3,5-di-tert-butyl-2-hydroxybenzyl)-benzene-1,2-diamine.[17] 1,10-Phenanthroline-1,2-diamine[20] (10 mmol), 2,4-di-tert-butyl-6-(chloromethyl)phenol (30 mmol), and triethylamine (30 mmol) were

(10) (a) Chaudhuri, P.; Wieghardt, K. *Prog. Inorg. Chem.* **2001**, *50*, 151−216. (b) Lahti, P.M. In *Magnetic Properties of Organic Materials*; Lahti, P. M., Ed.; Marcel Dekker: New York, 1999; pp 661−699. (c) Schultz, D. A. In *Magnetic Properties of Organic Materials*; Lahti, P. M., Ed.; Marcel Dekker: New York, 1999; pp 103−125.
(11) (a) Gateschi, D.; Rey, P. In *Magnetic Properties of Organic Materials*; Lahti, P. M., Ed.; Marcel Dekker: New York, 1999, pp 601−627. (b) Stroh, C.; Turek, P.; Rabu, P.; Ziessel, R. *Inorg. Chem.* **2001**, *40*, 5334.
(12) Buttner, T.; Geier, J.; Frison. G.; Harmer, J.; Calle, C.; Schweigel, A.; Schonberg, H.; Grutzmacher, H. *Science* **2005**, *307*, 235.
(13) Caneschi, A.; Gatteschi, D.; Sessoli, R.; Rey, P. *Acc. Chem. Res.* **1989**, *22*, 392.
(14) Pierpont, C. G.; Lange, C. W. *Prog. Inorg. Chem.* **1994**, *41*, 331−442.
(15) Adam, D.; Dei, A.; Rheingold, A. L.; Hendrickson, D. N. *J. Am. Chem. Soc.* **1993**, *115*, 8221.
(16) Gordon-Wylie, S. W.; Claus, B. L.; Horwitz, C. P.; Leychkis, Y.; Workman, J. M.; Marzec, A. J.; Clark, G. R.; Rickard, C. E. F.; Conklin, B. J.; Sellers, S.; Yee, G. T.; Collins, T. J. *Chem.—Eur. J.* **1998**, *4*, 2173.
(17) Aukauloo, A.; Ottenwaelder, X.; Ruiz, R.; Poussereau, S.; Pei, Y.; Journaux, Y.; Fleurat, P.; Volatron, F.; Cervera, B.; Muñoz, M. C. *Eur. J. Inorg. Chem.* **1999**, *7*, 1067.
(18) Lanznaster, M.; Hratchian, H. P.; Heeg, M. J.; Hryhorczuk, L. M.; McGarvey, B. R.; Schlegel, H. B.; Verani, C. N. *Inorg. Chem.* **2006**, *45*, 955.
(19) Gagne, R.; Koval, C.; Licenski, G. *Inorg. Chem.* **1980**, *19*, 2854

refluxed for 48 h in dichloromethane. The reaction solution was washed 3 times with water and dried over Na_2SO_4, and the solvent was removed by rotatory evaporation. The remaining yellowish viscous oil was dissolved in ethanol and kept at 0 °C for 24 h. A colorless crystalline precipitate was formed. Yield: 80%. ESI: m/z^+ 865.23, 100% for $[C_{57}H_{76}N_4O_3 + H^+]$. Anal. Calcd for $C_{57}H_{76}N_4O_3$·EtOH: C, 77.76; H, 9.07; N, 6.15. Found: C, 77.75; H, 9.16; N, 6.11. ^{1}H NMR (300 MHz, $CDCl_3$): δ 8.55 (s, 1H), 7.32 (dd, 2H), 7.15 (d, 1H), 7.07 (dd, 2H), 7.03 (dd, 2H), 7.95 (d, 3H), 6.87 (t, 1H), 4.39 (d, 1H), 4.29 (d, 2H), 4.19 (d,1H), 3.92 (d, 2H), 1.45 (s, 9H), 1.29 (s, 18H), 1.24 (s, 9H), 1.03 (s, 18H). IR (KBr pellet, cm^{-1}): 3345(m) ν(N−H); 2956(m), 2912(m), 2870(m), ν(C−H); 1592(s), 1568(w) 1482(m), 1458(s), 1427(s), 1391(s), 1361(s), ν(C═C); 1232(s), ν(C−O).

[Fe^{III}L^2]·$^1/_2$MeCN. The ligand **H$_3$L^1** (0.5 mmol) was dissolved in anhydrous methanol and treated with $NaOCH_3$ (1.5 mmol) under argon. $FeCl_3$ (0.5 mmol) was added to the resulting solution, and the mixture was heated at 50 °C and stirred for 30 min. The solvent was removed by rotatory evaporation, forming a dark brown precipitate of **[Fe^{III}L^1]**. ESI: m/z^- 916.4, 100% for $[C_{57}H_{73}N_4O_3Fe - H^+]$. IR (KBr pellet, cm^{-1}): 2954(s), 2905(m), 2863(m), ν(C−H); 1576(s), 1533(s), 1465(s), 1439(s), 1416(s), 1386(s), 1362(s), ν(C═C); 1270(s), 1252(s), 1236(s), ν(C−O).

The recrystallization of **[Fe^{III}L^1]** in MeCN/ethyl ether (1:2) yielded **[Fe^{III}L^2]·$^1/_2$MeCN** as an X-ray suitable crystalline solid. ESI: m/z^+ 916.5, 100% for $[C_{57}H_{71}N_4O_3Fe + H^+]$. Anal. Calcd for $C_{57}H_{71}N_4O_3Fe$: C, 74.74; H, 7.81; N, 6.12%. Found: C, 74.80; H, 7.58; N, 5.97%. IR (KBr pellet, cm^{-1}): 2954(s), 2903(m), 2867(m), ν(C−H); 1610(m), ν(C═N); 1578(s), 1530(s), 1469(s), 1441(s), 1418(s), 1388(s), 1359(s), ν(C═C); 1269(s), 1254(s), 1239(s), ν(C−O).

[Fe^{III}(L^2)Cu^{II}(Cl)$_2$(MeOH)]. This complex was synthesized by the reaction between **[Fe^{III}L^1]** or **[Fe^{III}L^2]·$^1/_2$MeCN** (0.5 mmol) and $CuCl_2$·$2H_2O$ (1 mmol) in methanol at 50 °C for 1 h under stirring. After removal of the solvent by rotatory evaporation, the remaining solid was dissolved in dichloromethane and filtered to remove any unreacted material. Methanol (1:2) was added to the filtrate. Slow evaporation of the solvent in this solution gave a crystalline precipitate suitable for X-ray diffraction. ESI: m/z^+ 505.2, 100% for $[C_{57}H_{71}N_4O_3CuFe{\cdot}CH_3OH]^{2+}$; 1013.2, 40% for $[C_{57}H_{71}N_4O_3ClCuFe]^+$; 1045.2, 25% for $[C_{57}H_{71}N_4O_3ClCuFe{\cdot}CH_3OH]^+$. Anal. Calcd for $C_{58}H_{75}Cl_2CuFeN_4O_4$: C, 64.35; H, 6.98; N, 5.18%. Found: C, 64.26; H, 7.02; N, 5.26%. IR (KBr pellet, cm^{-1}): 2956(s), 2905(m), 2868(m), ν(C−H); 1609(m), ν(C═N); 1574(s), 1529(s), 1470(s), 1423(s), 1388(s), 1360(s), ν(C═C); 1267(s), 1251(s), ν(C−O).

X-ray Structural Determinations. Diffraction data were collected on a Bruker P4/CCD diffractometer equipped with Mo radiation and a graphite monochromator at −65 °C for **2** and −60 °C for **3** (Table 1). For each collection, a sphere of data was measured at 10 s/frame and 0.2° between frames. The frame data was indexed and integrated with the SMART, SAINT, and SADABS software.[21] All structures were refined using Sheldrick's SHELX-97 software.[22] Compound **2** crystallized as dark square rods of $[Fe(C_{57}H_{71}N_4O_3)]$·$^1/_2(CH_3CN)$. A 0.3 × 0.2 × 0.2 mm^3 sample was used for data collection. A total of 1850 frames were collected, yielding 15 010 reflections, of which 11 997 were independent. Hydrogen positions were calculated. Typical *t*-butyl disorder was observed. In the case of C12−C14, partial atomic occupancies were used, and the thermal parameters for these partial atoms were held isotropic. The solvent was included on the inversion center in the model using the SQUEEZE software of PLATON.[23] Compound **3** crystallized as dark plates of $[Fe(C_{58}H_{75}N_4O_4Cl_2)Cu]{\cdot}2CH_3OH$. A 0.16 × 0.12 × 0.06 mm^3 sample was used for data collection. A total of 1850 frames were collected, yielding 16 712 reflections, of which 13 343 were independent. Hydrogen positions were calculated or observed. The methanol solvent electrons were placed by use of Spek's SQUEEZE portion of the PLATON software.

Table 1. Crystal Data

	2	**3**
formula	$C_{58}H_{72.5}$**Fe**$N_{4.5}O_3$	$C_{60}H_{83}Cl_2$**CuFe**N_4O_6
fw	936.55	1146.59
space group	$P\bar{1}$	$P\bar{1}$
a (Å)	13.3191(15)	13.049(7)
b (Å)	14.8139(18)	15.470(7)
c (Å)	15.9524(18)	16.613(9)
α (deg)	113.382(3)	93.584(17)
β (deg)	92.588(4)	95.480(7)
γ (deg)	94.931(2)	108.102(8)
V (Å^3)	2867.5(6)	3158(3)
Z	2	2
temp (K)	208(2)	213(2)
λ (Å)	0.71073	0.71073
density, calcd (g cm^{-3})	1.085	1.206
μ (mm^{-1})	0.306	0.699
R(*F*)[a] (%)	6.54	7.73
wR(*F*)[a] (%)	17.93	16.67

[a] $R(F) = \sum||F_o| - |F_c||/\sum|F_o|$ for $I > 2\sigma(I)$; $wR(F) = [\sum w(F_o^2 - F_c^2)^2/\sum w(F_o^2)^2]^{1/2}$ for $I > 2\sigma(I)$.

Results and Discussion

Ligand Design. From the electroactive ligands mentioned above, catechols and nitronyl-nitroxides are good spin carriers, but their synthetic manipulations are far from trivial. Similarly, ligands able to generate verdazyl radicals show limited coordination capability, often restricted to Cu(I) centers. On the other hand, substituted phenols coordinate to practically every transition or main-group metal ion and generate phenoxyl radical-containing complexes. Because of their synthetic flexibility and ease of radical generation when associated with lower symmetries, these are the most convenient electroactive groups for the study of radical/metal interactions. In searching for ways of designing ligands that foster lower symmetries for radical stabilization, we used the approach described by Sato[24] to obtain *N*,*N*,*N*′-trisubstituted aromatic diamines. The reaction of phenanthroline-diamine with excess of 2,4-di-*tert*-butyl-6-(chloromethyl)-phenol gave the new N_2O_3 triphenolic ligand **H$_3$L^1**. This ligand resembles previous mononucleating ligands used for biomimetic modeling[25,26] but displays a phenanthroline

(20) (a) Yamada, M.; Tanaka, Y; Yoshimoto, Y.; Kuroda, S.; Shimao, I. *Bull. Chem. Soc. Jpn.* **1992**, *65*, 1006. (b) Bodige, S.; MacDonnell, F. M. *Tetrahedron Lett.* **1997**, *38*, 8159.
(21) *APEX II*, *SMART*, *SAINT*, and *SADABS*; Bruker AXS Inc.: Madison WI.
(22) Sheldrick, G. *SHELX-97*; University of Göttingen: Göttingen, Germany, 1997.
(23) (a) Spek, A. L. *PLATON*; Utrecht University: Utrecht, The Netherlands, 2003. (b) Spek, A. L. *J. Appl. Crystallogr.* **2003**, *36*, 7−13.
(24) Sato, M.; Mori, I.; Iida, T. *Synthesis* **1992**, 539.
(25) Colpas, G. J.; Hamstra, B. J.; Kamps, J. W.; Pecoraro, V. L. *Inorg. Chem.* **1994**, *33*, 4669.
(26) Schmitt, H.; Lomoth, R.; Magnuson, A.; Park, J.; Fryxelius, J.; Kritikos, M.; Martensson, J.; Hammarstrom, L.; Sun, L.; Akermark, B. *Chem.—Eur. J.* **2002**, *08*, 3757.

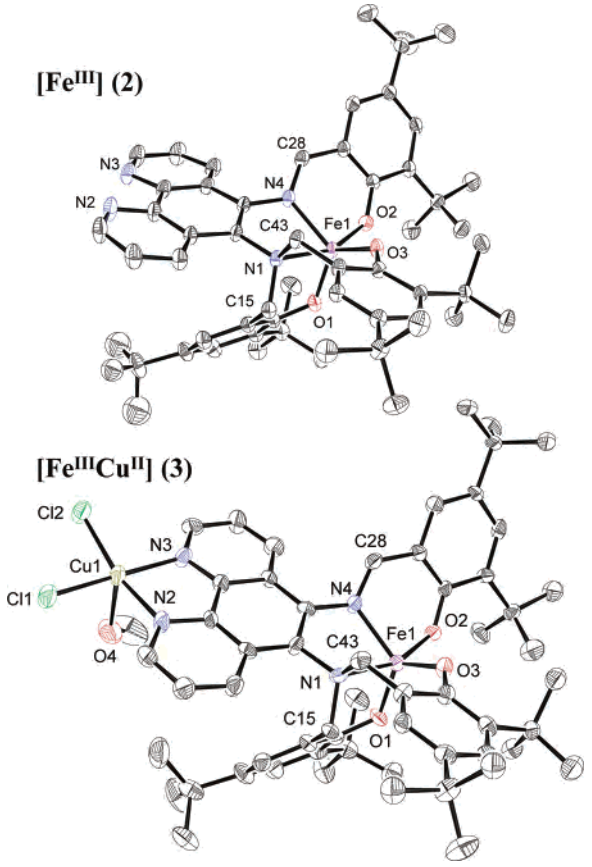

Figure 1. ORTEP drawings for **2** and **3**.

moiety that favors softer ions, such as Cu(II), and an N_2O_3 pocket including three phenol-containing arms that supports harder trivalent ions such as Fe(III).

Complex Synthesis. Treatment of $\mathbf{H_3L^1}$ with $FeCl_3$ in dry methanol under argon resulted in the five-coordinated species $[Fe^{III}L^1]$ **(1)**. Aerobic crystallization in Et_2O/MeCN (2:1) yields $[Fe^{III}L^2]\cdot{}^1/_2$MeCN **(2)**, and its X-ray structure (Figure 1 top) indicates that oxidation of the coordinated ligand $(L^1)^{3-}$ takes place at the C−N bond of the protonated amine nitrogen atom. The conversion mechanism is under investigation. Copper chloride reacts with **1** (or **2**) in MeOH yielding the heterobimetallic species $[Fe^{III}(L^2)Cu^{II}(Cl)_2(MeOH)]$ **(3)**. Scheme 2 shows the ligand and complex syntheses.

Molecular Structures. The crystal structures for the Fe-containing **2** and the Cu/Fe-containing **3** were solved, and the crystallographic data are summarized in Table 2. We will restrict our crystallographic discussion to **3**, because the former compound shows chemically equivalent structural features in absence of the copper ion. The ORTEP representation for **3** is given in Figure 1 with selected bond lengths and angles. The overlap of the least-squares fit of both complexes is added in the Supporting Information **(**Figure S1**)** and demonstrates the similar nature of both structures. This neutral complex confirms the identity of the ligand as being formed by a 5,6-diamino-1,10-phenanthroline moiety showing a monosubstituted amine N1 with one group 2,4-di-*tert*-butyl-6-methylphenol N,N appended, whereas the vicinal amine N4 exhibits two of these groups. The short

Table 2. Selected Bond Lengths (Å) and Angles (deg) for **2** and **3**

	2	**3**
Fe−O1	1.853(2)	1.837(4)
Fe−O2	1.916(2)	1.910(4)
Fe−O3	1.873(2)	1.865(4)
Fe−N1	2.307(2)	2.284(5)
Fe−N4	2.043(2)	2.029(5)
Cu−N3		2.040(5)
Cu−Cl1		2.254(2)
Cu−Cl2		2.236(2)
Cu−O4		2.307(7)
N1−C15	1.500(3)	1.522(7)
N1−C43	1.498(4)	1.506(8)
N4−C28	1.315(3)	1.326(8)
O1−Fe−O2	103.9(1)	101.1(2)
O1−Fe−O3	120.4(1)	118.4(2)
O2−Fe−O3	97.0(1)	99.2(2)
O1−Fe−N4	115.2(1)	120.1(2)
O3−Fe−N4	121.6(1)	118.7(2)
O2−Fe−N4	85.6(1)	86.3(2)
O1−Fe−N1	89.8(1)	91.3(2)
O3−Fe−N1	88.8(1)	87.5(2)
O2−Fe−N1	159.4(1)	160.7(2)
N4−Fe−N1	74.6(1)	74.7(2)
N2−Cu−N3		80.6(2)
N2−Cu−Cl2		165.9(2)
N3−Cu−Cl2		92.3(2)
N2−Clu−Cl1		92.6(2)
N3−Cu−Cl1		170.8(2)
Cl2−Cu−Cl1		92.9(1)
N2−Cu−O4		91.4(3)
N3−Cu−O4		89.2(3)
Cl2−Cu−O4		100.7(2)
Cl1−Cu−O4		97.2(2)
Cu ··· Fe		8.097(2)

C28−N4 bond length is characteristic of a C═N imine bond and establishes the locus of the ligand oxidation. Both metal ions present are five-coordinated and present a distance of ∼8.0 Å. The copper center is coordinated to the nitrogen atoms N(2) and N(3) of the phenanthroline. This forms the base of a square pyramid with two chloride ions trans to the nitrogen atoms and a molecule of methanol occupying the apical position. The iron center is coordinated to each of the three oxygen atoms of the phenolate groups O1, O2, and O3 and to the nitrogen atoms N1 and N4 in a distorted trigonal bipyramidal[27] geometry, similar to that observed for **2**.

Electrochemistry. Cyclic voltammograms were taken for **2** and **3** to assess redox potentials needed for ground state switching and to evaluate the changes caused by insertion of the Cu(II) ion into the latter compound **(**Figure 2). All potentials are reported versus the Fc^+/Fc couple. A one-electron reversible process for the couple Fe(III)/Fe(II) is seen at −1.35 V for **2**, whereas two quasireversible processes attributed to the phenolate/phenoxyl couple are observed at 0.63 and 0.81 V in **2**. Similarly, the metal-centered reduction is observed at −1.21 V for **3**, with a ligand-centered oxidation seen at 0.69 V for **3**. Both compounds are in good agreement for these processes, and the main difference relates to a new set of ill-defined waves attributed to the Cu(II) center and appearing at $E_{pc} = -0.38$, $E_{pc} = -0.55$, $E_{pa} = -0.27$, and $E_{pa} = 0.15$ V. The low reversibility of these

(27) $\tau = 0.63$ for Fe(III) and 0.08 for Cu(II), see: Addison, A. W.; Rao, T. N. *J. Chem. Soc. Dalton Trans.* **1984**, 1349.

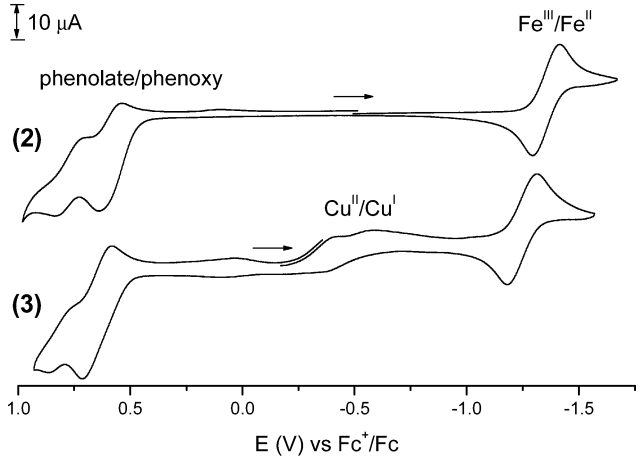

Figure 2. Cyclic voltamograms of **2** (a) and **3** (b) at 1×10^{-3} mol L^{-1} in dichloromethane with 0.1 mol L^{-1} of $TBAClO_4$ at 100 mV s^{-1}, using a three-electrode system: C = working, Ag/AgCl = reference and Pt = auxiliary. Ferrocene was used as an internal standard ($E_{1/2}$ = 530 mV vs Ag/AgCl).

processes is the result of the presence of three monodentate ligands and related to conformational transitions and geometrical differences between the Cu(I) and Cu(II) ions.[28] We suggest that upon reduction at least one of the chloride groups leaves to accommodate the preferred tetrahedral geometry for Cu(I). Bulk electrolysis was performed on **3** to characterize the changes in ground state associated with oxidations or reductions. Oxidative electrolysis at 0.90 V vs Fe^+/Fe and reductive electrolysis at −1.0 V vs Fc^+/Fc were performed aiming at the formation of phenoxyl radicals and the reduction $Cu^{II} \rightarrow Cu^{I}$, respectively. The resulting solutions were analyzed by EPR spectroscopy.

Magnetic Properties. To characterize the magnetic behavior of **2** and each of the possible states originated by the application of selective potentials to **3**, we performed a series of experiments involving magnetic susceptibility and EPR techniques. The EPR spectrum of **2** in CH_2Cl_2 at 120 K shows a broad signal in the region of 700−1600 G (Figure 3, top) and will be shown below to support a large anisotropic ligand field such as that found in a five-coordinate high spin Fe^{III} center. The EPR spectrum is derived from the spin Hamiltonian[29]

$$H = \beta(BgS) + D(S_z^2 - (35/12)) + E(S_x^2 - S_y^2) + B_4^0 O_4^0 + B_4^2 O_4^2 + B_4^4 O_4^4 \quad (1)$$

for an $S = 5/2$ system. The term B is the magnetic field, and the terms D and E are zero-field parameters with D being nonzero for symmetries lower than tetrahedral or octahedral and E being restricted to magnitudes equal or smaller than one-third of $|D|$. The zero field O_4^m terms are functions of the spin operators S to the forth power, and the B_4^m terms are constants obtained from experimental data. The g value is normally isotropic and close to 2.0. Simulations were attempted for the EPR spectrum of **2**; however, the presence

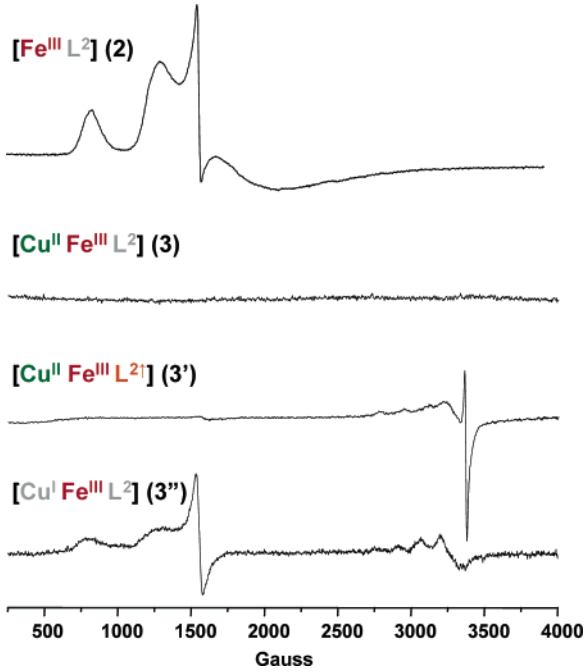

Figure 3. EPR spectra obtained from **2** (top) and **3** in its resting state, upon ligand oxidation (**3′**) and Cu(II) reduction (**3″**).

of five adjustable parameters in the spin Hamiltonian and the large magnitude of D relative to the Zeemann interaction makes it impossible to obtain a good simulation in a reasonable length of time. Nonetheless, these attempts clearly indicate that the term D must be greater than 0.3 cm^{-1}, the spectrometer frequency, and the term E must be nearly one-third of the D value ($|D| > 0.3$ cm^- and $E \approx |D|/3$) to explain why the only visible part of the spectrum is found in the region of 700−1600 G. Similar EPR spectra with the Fe(III) center in highly anisotropic sites are known in the literature.[30,31] However, we have included a series of simulations in the Supporting Information (Figures S2−S4) to show how the above conclusions about D and E can be obtained. The large magnitude of both D and E indicate that the ligand field about Fe(III) must be very anisotropic, which would certainly be true for the proposed five-coordination. It is evident from the molecular structures that this five-coordination is retained in **3**, and so, one would expect that the $Fe(III)_{hs}$ center ($S_{Fe} = 5/2$) will interact with the Cu(II) ion $S_{Cu} = 1/2$.

The observed EPR spectrum of **3** is shown in Figure 3 **(3)** and is silent. If the exchange interaction between the Fe(III) and Cu(II) were large compared to the Zeemann interaction and the zero-field interaction of the Fe(III) ion, the ground state would be an antiferromagnetic ($S_{Fe-Cu} = 2$) state or a ferromagnetic ($S_{Fe+Cu} = 3$) state. Such integer states are often referred to as being silent in EPR, but this is not always true; they are silent only in the X band when D is large compared to the Zeemann interaction and the available magnetic field sweep in the spectrometer is not too large. To evaluate this premise, the magnetic susceptibility for **3**

(28) Villeneuve, N. M.; Schroeder, R. R.; Ochrymowycz, L. A.; Rorabacher, D. B. *Inorg. Chem.* **1997**, *36*, 4475.
(29) Abragam, A.; Bleaney, B. *Electron Paramagnetic Resonance of Transition Ions*; Dover Publications, Inc.: New York, 1986.
(30) Dowsing, R. D.; Gibson, J. F. *J. Chem. Phys.* **1969**, *50*, 290
(31) Golding, R. M.; Singhasuwich, T.; Tennant, W. C. *Mol. Phys.* **1977**, *34*, 1343.

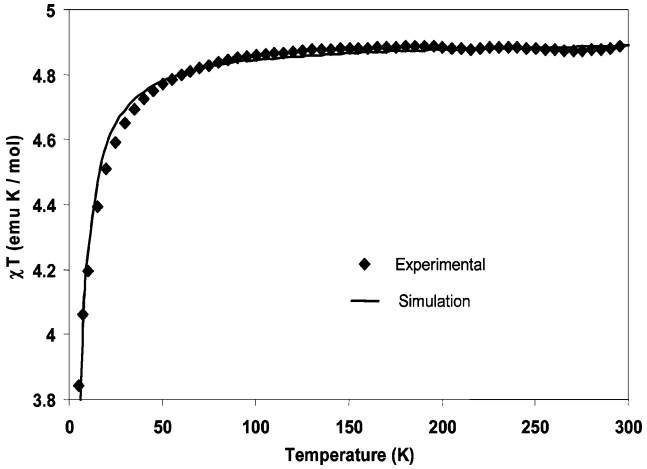

Figure 4. Magnetic susceptibility data for **3**.

was taken from 300 to 4 K. The curve seen in Figure 4 resembles that for an antiferromagnetically coupled core. Nonetheless, χT starts at around 4.88 emu K mol^{-1} at 300 K and continues in a plateaulike behavior down to 50 K, where $\chi T = 4.79$ emu K mol^{-1}. These values are very close to the expected sum of two independent spins, 5/2 and 1/2, and thus are indicative of weakly coupled or uncoupled spins. Below 50 K, the χT values decrease reaching a value of 3.83 emu K mol^{-1}. Fitting of the curve using an average g value of 2.03 in the expression[2] derived from the Hamiltonian, $H = -2JS_AS_B$, yields a coupling constant J between -1.0 and -2.0 cm^{-1} related to an $S = 2$ ground state.

$$\chi T = \frac{3}{3} g_{av}{}^2 \frac{10 + 28e\frac{6J}{kT}}{5 + 7e\frac{6J}{kT}} \qquad (2)$$

The weak interaction observed for **3** is likely to be the result of the long distance of ~8 Å, as well as of the superexchange pathways related to both metal ions exhibiting local five-coordinate geometries.

Although the magnetic susceptibility indicates a small magnitude for the J coupling parameter, the fact that a silent EPR spectrum was observed for **3** means the J value is not zero and must be of a magnitude similar to that of the Zeemann, zero-field, or both interactions. To address this issue, EPR simulations of the expected spectra for J values in this range were run,[32] considering both antiferromagnetic and ferromagnetic values for the J interaction, and are shown in Figure 5. The red central line considers absence of coupling and therefore has a $J = 0$. Below this line in the figure, antiferromagnetic coupling is considered with J values being increased from 0.05 to 0.50 cm^{-1} by increments of 0.05 cm^{-1}, whereas the part of the figure above the red line shows similar increments in a ferromagnetic coupling. The calculation used $g_{||} = 2.20$ and $g_{\perp} = 2.05$ for the Cu(II) ion and $g = 2.0$, $D = 0.4$ cm^{-1}, and $E = 0.133$ cm^{-1} for the Fe(III) ion. The inclusion of the hyperfine interactions for Cu(II) did not show significant improvements. Very weak

(32) Software by B. R. McGarvey. Ferromagnetic interactions are defined as negative J values, and hyperfine interactions are disregarded.

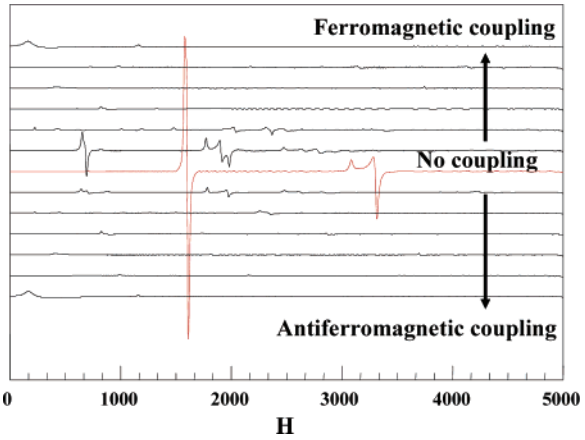

Figure 5. Simulated EPR spectra for weakly coupled Cu(II) and Fe(III) centers at different J values.

couplings of 0.15 cm^{-1} suffice to yield a nearly silent spectrum. It should be noted that there are still smaller intensity signals in these simulations. These signals would not be seen if we were to increase the line widths. Dipolar interactions between the two metal ions, which are about 8 Å apart, would at least double the line widths used in our simulations. If there is a spin-exchange interaction operating by spin transfer through the ligand, this exchange interaction could be strongly coupled to the phonon system leading to short T_1 values that would broaden these lines beyond the limits of detection by EPR. Furthermore, it is likely that the spin-exchange parameter is not isotropic as assumed. All or only some of these reasons can explain the absence of EPR signal. However, it must be repeated that despite our inability to pinpoint the exact reasons for the lack of EPR signal, this has to be caused by the existence of an exchange interaction between the two metal ions, and this interaction is much stronger than the direct dipolar interaction (~0.001 cm^{-1}). Future experiments aimed at understanding weakly coupled cores in similar scaffolds will include EPR spectroscopy at lower temperatures, higher magnetic fields, and higher spectrometer frequencies and will deal with series of complexes where the Cu(II) ion is replaced by centers with a larger spin, such as bivalent chromium, iron, or cobalt. The susceptibility response of the coupled core in these new complexes, especially at low temperatures, will give more pronounced results.

After oxidative electrolysis of **3** at 0.90 V vs Fc^+/Fc, the resulting EPR spectrum **(**Figure 3 **(3′))** shows a sharp, symmetrical, free-radical signal at $g = 2.00$ on top of a typical Cu(II) spectrum with $g_{\perp} < g_{||}$ and $A_{||} > A_{\perp}$ for an unpaired electron occupying the $d_{x^2-y^2}$ orbital of the Cu(II) center.[33] The free-radical signal was simulated and then subtracted to give the Cu(II) spectrum shown in Figure 6 (top). The intensity of the signal for the free radical was only 2% of the Cu(II) spectrum. The simulated spectrum gave spin Hamiltonian parameters of $g_{||} = 2.22$, $g_{\perp} = 2.04$, $A_{||} = 168$ G, and $A_{\perp} = 25$, thus supporting a covalently bound Cu(II) ion. There is a very small signal in the region of $g =$

(33) Solomon, E. I.; Gewrith, A. A.; Westmoreland, T. D. In *Advanced EPR, Applications in Biology and Biochemistry*; Hoff, A. J., Ed.; Elsevier: Amsterdam, 1989; Chapter 25.

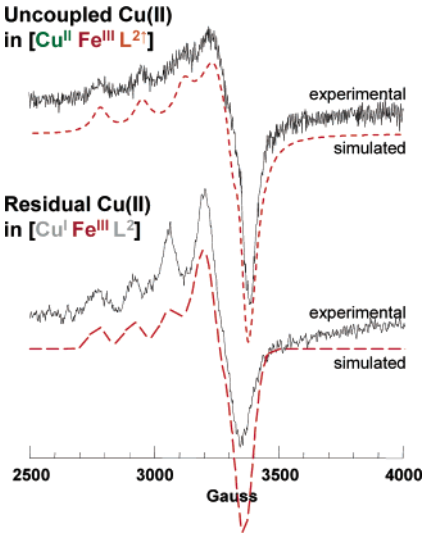

Figure 6. Experimental and simulated data for the copper(II) signals in spectra **3′** and **3″**.

4 that is attributed to trace amounts of ferric impurity, possibly from **2**. The absence of a strong Fe(III) signal could be explained by assuming the formation of a phenoxyl radical strongly coupled to the Fe(III) center, whose resonance cannot be detected. In this case, a strongly coupled $S = 2$ ground state is formed with a large zero-field interaction that makes it impossible to detect any resonance in the magnetic field studied. Apparently, the formation of the phenoxyl radical destroys any spin coupling to the Cu(II) ion. Simulations for the copper ion used the spin Hamiltonian in eq 3. The powder spectrum of Cu(II) is generally found in the 2000−3500 G region of the EPR spectrum with $g_{\|} > g_{\perp} > 2.0$ and $|A_{\|}| > |A_{\perp}|$.

When electrolysis was performed at −1.0 V vs Fc^{+}/Fc, the reduction Cu(II) + $e^{-} \rightarrow$ Cu(I) was expected, leaving an Fe(III) spectrum similar to that obtained for **2**. An additional residual spectrum resembling that of a Cu(II) ion is also observed, suggestive of incomplete electrolysis (Figure 6**,** bottom). Simulation of this Cu(II) signal gives $g_{\|} = 2.23$, $g_{\perp} = 2.03$, $A_{\|} = 143$ G, and $A_{\perp} \approx 30-40$ G, confirming its origin in a Cu(II) ion. The differences between the hyperfine values for the two Cu(II) spectra indicate that the environments are both covalent but not identical.

Conclusions

This article describes the design of new molecular scaffolds for multispin complexes, based on a novel binucleating ligand, where the coordinated metals exhibit unusual geometries that stabilize radical formation. Selective redox response was achieved upon oxidation or reduction of distinct components of these complexes and may be useful to the development of magnetic modulation in approaches for multicomponent surface chemistry. Further improvements are necessary to define the possibilities and limitations of these systems. Well-behaved one-electron oxidations and reductions are needed for precise modulation and switching and may lead to the use of different metal centers and organic groups capable of radical stabilization. Similarly, replacement of the monodentate ligands coordinated to Cu(II) ions are currently under investigation. Similar complexes with chelates coordinated to the copper ion for a better electrochemical reversibility have been isolated, as shown in Scheme 3, and step further toward the functionalization of anchoring groups for surface deposition. It is our hope that this research will contribute to the broader understanding of the mechanisms involved in magnetic modulation and switching.

Scheme 3 [a]

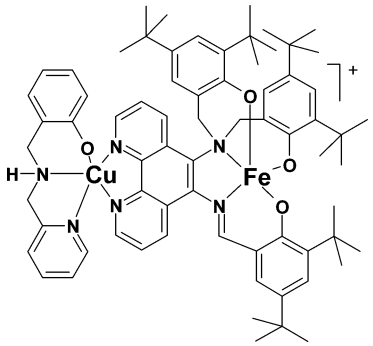

[a] $m/z^{+} = 1191.4$ for $[M]^{+}$.

Acknowledgment. This paper is dedicated to Professor Phalguni Chaudhuri for his contribution to the fields of modular synthesis and magnetism of multinuclear systems. C.N.V. thanks Wayne State University, the Donors of the ACS-PRF (Grant 42575-G3), and the Nano@Wayne Initiative (Grant 11E420), and G.T.Y. acknowledges the NSF (Grant CHE-023488) for financial support. We acknowledge Professor E. Rentschler, University of Mainz, for initial magnetic susceptibility measurements, Dr. A. Ozarowski, Florida State University, and Dr. H. Weihe, University of Copenhagen, for some of the EPR simulation programs.

Supporting Information Available: Overlap of the least-squares fits for **2** and **3** (PDF) and X-ray crystallographic data (CIF). This material is available free of charge via the Internet at http://pubs.acs.org.

IC060944A